

# Gravitational waves from equatorially eccentric extreme mass ratio inspirals around swirling Kerr black holes

Yuhang Gu<sup>1</sup>, Songbai Chen<sup>1,2\*</sup>, Jiliang Jing<sup>1,2 †</sup>

<sup>1</sup>*Department of Physics, Institute of Interdisciplinary Studies,  
Key Laboratory of Low Dimensional Quantum Structures and Quantum Control of Ministry of Education,  
Synergetic Innovation Center for Quantum Effects and Applications,  
Hunan Normal University, Changsha, Hunan 410081, People's Republic of China*

<sup>2</sup>*Center for Gravitation and Cosmology, College of Physical Science and Technology,  
Yangzhou University, Yangzhou 225009, People's Republic of China*

## Abstract

We have studied the gravitational wave generated by extreme mass ratio inspirals (EMRIs) along eccentric orbits on equatorial plane within the frame of the swirling-Kerr black hole spacetime. The swirling-Kerr black hole has an extra swirling parameter, which characterizes the rotation of universe background. Our findings indicate that this swirling parameter leads to a delay phase shift in the gravitational waveforms. The impact of the swirling parameter on EMRI gravitational waves is suppressed by the black hole's spin parameter. As a result, extracting information about the swirling parameter from gravitational waves in a static black hole spacetime is much easier than in the case of a rapidly rotating black hole. Our analysis also shows that a high black hole spin leads to a greater overlap of gravitational waveforms for different swirling parameters. We further investigate the potential issue of waveform confusion caused by the orbital eccentricity and semi-latus rectum parameters. As the swirling parameter increases, the relative variation in eccentricity also increases, while the variation in the semi-latus rectum decreases rapidly. The trends in these changes with the swirling parameter resemble those observed with the MOG (Modified Gravity) parameter, though with different rates of change. These results provide deeper insights into the properties of EMRI gravitational waves and the swirling of the universe background.

PACS numbers: 04.70.Cs, 98.62.Mw, 97.60.Lf

---

\* Corresponding author: csb3752@hunnu.edu.cn

† jljing@hunnu.edu.cn

## I. INTRODUCTION

Gravitational wave astrophysics has been entered into a completely new era due to the direct detections of hundreds of gravitational wave events [1–3]. Among various sources of gravitational waves, EMRI systems [4–19] are of particular interest to future space-based gravitational wave detectors [20–26] because their gravitational waves are in the lower frequency band [27–31] which are difficult to be explored by the current ground-based detectors. In the EMRI system, a stellar-mass object (the secondary with mass  $\mu$ ) slowly spirals inward the central supermassive black hole (the primary with mass  $M$ ) due to the gravitational emission, and undergoes numerous orbits before ultimate plunging. During its evolution, the gravitational waveforms generated by EMRIs are closely related to the trajectory of the smaller object, which imprints characteristic information on the spacetime geometry around the supermassive black hole. This means that EMRI gravitational waves provide invaluable probes to study the properties of supermassive black holes and to examine gravitational theories. EMRI gravitational waves have extensively applied to constrain the nature of Kerr spacetime [32–35], and to test theories of gravity include Einstein’s general relativity, the Brans-Dicke theory [36–38], and dynamical Chern-Simons gravity [39–41] as well as quantum gravity [42–44]. Recently, EMRI gravitational waves have also served as a power tool to detect dark matter around supermassive black holes [45–47] and to probe scalar charges induced by the dipole radiation [48–57]. EMRI gravitational waves can be used as standard sirens to investigate the expansion history of the universe, and further to constrain cosmological parameters [58].

Considering that all compact objects in the universe are rotating, it is natural to think that the rotation is a universal phenomenon which may also apply to the global universe. Recently, an exact solution for the Kerr black hole in a swirling universe was obtained by Astorino *et al* [59] through exploiting the Ernst formalism [60, 61] with a transformation embedding a Kerr seed spacetime into a rotating background. This black hole is a vacuum solution of Einstein field equation and is characterized by three parameters: black hole mass and spin parameters, as well as the swirling parameter. The swirling parameter describes the rotation of background universe, which can be interpreted as a gravitational whirlpool. The spin-spin interaction between the black hole and the background frame dragging results in the breaking of symmetry of spacetime geometry due to an additional force acting on the axis. Especially, the swirling-Kerr black hole is co-rotating with the swirling background in one hemisphere and counter-rotating in the other since the black hole spin does not affect its sign with respect to the equatorial plane. The breaking of symmetry leads to the non-

removable conical singularities along the symmetry axis, which means that there exists a cosmic string or a strut to compensate the force effect induced by the spin-spin interaction. The swirling-Kerr black hole solution possesses two horizon surfaces located at  $r_{\pm} = M \pm \sqrt{M^2 - a^2}$ , which is independent of the swirling parameter and equivalent to the Kerr case. However, that the background swirling deforms the horizon geometry [59]. In this swirling-Kerr black hole spacetime, there is no closed time-like curves which means that it is less exotic than the Gödel or the Taub-NUT spacetime [59]. The geodesic in the swirling universe is found to no longer be decoupled because the spacetime is no longer of Petrov type  $D$ , which could yield chaotic motion of particles in this spacetime [62, 63]. Moreover, the swirling parameter is found to drive the light rings outside the equatorial plane, which results in that the contour of the shadow becomes a tilted oblate shape [64]. Recent studies analyzed the geometrically thick equilibrium tori orbiting a Schwarzschild black hole in swirling universes [65] and a Kerr black hole in swirling [66] universes respectively, and explored new effects arising from background swirling on the equilibrium tori around the black hole. The studies of the swirling black holes have been generalized to the electromagnetic case [67, 68]. These studies shed new light on understanding black holes in swirling universe.

The main motivation of this paper is to study the gravitational waves from equatorially eccentric EMRIs around a swirling-Kerr black hole and to probe the corresponding effects from the background swirling. Considering a stellar-mass object moving along the equatorially eccentric orbits around a supermassive swirling black hole, we analyze the gravitational waveforms generated by this EMRI system through using the numerical Kludge scheme [69, 70] and discuss how the background swirling influence these waveforms. We further also analyzed the gravitational waveform confusion problem.

The plan of this paper is as follows: In the Sec.II, we briefly review the swirling-Kerr black hole solution [59] and the equatorial EMRI systems. In Sec.III, we present properties of EMRI gravitational waves in the swirling background and analyze effects of the swirling parameter as well as the black hole spin parameter. Finally, we present a summary.

## II. EQUATORIAL EMRI SYSTEM WITHIN THE FRAMEWORK OF SWIRLING KERR SPACETIMES

Lets us first briefly review the Kerr black hole solution embedded in a rotating universe background. It is a stationary, axially symmetric and non-asymptotically flat black hole solution of the vacuum Einstein equations, which can be obtained through an Ehlers transformation on the Kerr solution as a seed [59]. The

swirling Kerr black hole possesses the swirling parameter and the spin parameter, and its metric form in the Boyer-Lindquist coordinates can be written as

$$ds^2 = F(d\phi - \omega dt)^2 + F^{-1} \left[ -\rho^2 dt^2 + \Sigma \sin^2 \theta \left( \frac{dr^2}{\Delta} + d\theta^2 \right) \right], \quad (1)$$

where functions  $F$  and  $\omega$  can be expressed as a finite power series of the swirling parameter  $j$

$$F^{-1} = \chi_{(0)} + j\chi_{(1)} + j^2\chi_{(2)}, \quad \omega = \omega_{(0)} + j\omega_{(1)} + j^2\omega_{(2)}. \quad (2)$$

The expansion coefficients  $\chi_{(i)}$  and  $\omega_{(i)}$  are

$$\chi_{(0)} = \frac{R^2}{\Sigma \sin^2 \theta}, \quad \chi_{(1)} = \frac{4aM\Xi \cos \theta}{\Sigma \sin^2 \theta}, \quad \chi_{(2)} = \frac{4a^2 M^2 \Xi^2 \cos^2 \theta + \Sigma^2 \sin^4 \theta}{R^2 \Sigma \sin^2 \theta}, \quad (3)$$

and

$$\begin{aligned} \omega_{(0)} &= \frac{2aMr}{-\Sigma}, & \omega_{(1)} &= \frac{4 \cos \theta [-a\Omega(r-M) + Ma^4 - r^4(r-2M) - \Delta a^2 r]}{-\Sigma}, \\ \omega_{(2)} &= -\frac{2M\{3ar^5 - a^5(r+2M) + 2a^3 r^2(r+3M) - r^3(\cos^2 \theta - 6)\Omega + a^2[\cos^2 \theta(3r-2M) - 6(r-M)]\Omega\}}{\Sigma}, \end{aligned} \quad (4)$$

where

$$\begin{aligned} \Delta &= r^2 - 2Mr + a^2, & \rho^2 &= \Delta \sin^2 \theta, & \Sigma &= (r^2 + a^2)^2 - \Delta a^2 \sin^2 \theta, \\ \Omega &= \Delta a \cos^2 \theta, & R^2 &= r^2 + a^2 \cos^2 \theta, & \Xi &= r^2(\cos^2 \theta - 3) - a^2(1 + \cos^2 \theta). \end{aligned} \quad (5)$$

Here  $M$  and  $a$  denote respectively the mass parameter of the black hole and the angular momentum per unit mass. It reduces to the pure Kerr black hole as the swirling parameter  $j = 0$  and to the Schwarzschild black hole in swirling universes as the black hole spin  $a = 0$ . The spin-spin interaction between the black hole and the background dragging leads to a conical singularity along the symmetry axes [59], which deforms the horizon geometry and enhances the symmetry breaking regarding the spacetime properties. The presence of  $j$  yields that the north and south hemispheres of the swirling Kerr black hole rotate in opposite directions, which is different from that in the pure Kerr black hole case.

In the swirling Kerr black hole spacetime, the Lagrangian of a timelike particle moving along the geodesic is

$$\mathcal{L} = \frac{1}{2} g_{\mu\nu} \dot{x}^\mu \dot{x}^\nu. \quad (6)$$

This Lagrangian is independent of the coordinates  $t$  and  $\phi$ , which means that there are two conserved quantities for the timelike particle's motion along geodesics

$$E = -u_t = -g_{tt}u^t - g_{t\phi}u^\phi, \quad L_z = u_\phi = g_{t\phi}u^t + g_{\phi\phi}u^\phi, \quad (7)$$

where

$$u^t = \frac{F(E + L_z\omega)}{\rho^2}, \quad u^\phi = \frac{L_z}{F} - \frac{F\omega(E + L_z\omega)}{\rho^2}. \quad (8)$$

Here  $E$  and  $L_z$  correspond to the energy and the angular momentum of a particle, respectively. The timelike condition  $g_{\mu\nu}u^\mu u^\nu = -1$ , leads to a constraint condition for the particle's motion

$$h = g_{tt}\dot{t}^2 + g_{rr}\dot{r}^2 + g_{\theta\theta}\dot{\theta}^2 + g_{\varphi\varphi}\dot{\varphi}^2 + 2g_{t\varphi}\dot{t}\dot{\varphi} + 1 = 0. \quad (9)$$

Generally, this first-order differential equation is non-separable and there is no the Carter constant  $Q$  for the particle's motion. Therefore, we consider only the case where the particle's geodesics are limited in the equatorial plane and probe the corresponding effects of the swirling parameter on gravitational waves from extreme mass ratio inspirals.

For a bounded Kepler geodesic in the equatorial plane, the orbit can be characterized by the eccentricity  $e$  and the semi-major axis  $p$  with the forms

$$e = \frac{r_a - r_p}{r_a + r_p}, \quad p = \frac{2r_a r_p}{r_a + r_p}. \quad (10)$$

Here  $r_a$  and  $r_p$  respectively represent the apastron and periastron in the geodesic orbit. For the equatorial orbits, the eccentricity  $e$  and the semi-major axis  $p$  can be determined by particle's  $E$  and  $L_z$ . To circumvent numerical difficulties frequently related to turning points, one can transition the integration variable  $r$  to the angular coordinate  $\chi$  [69, 70]

$$r = \frac{p}{1 + e \cos \chi}. \quad (11)$$

As the parameter  $\chi$  transforms between 0 and  $2\pi$ , the coordinate  $r$  travels back and forth between the apastronic points  $r_a$  and  $r_p$ . The effective potential  $V_r$  for the geodesics in the equatorial plane is

$$V_r = -1 - \frac{L_z^2}{F} + \frac{F(E + L_z\omega)^2}{\rho^2}. \quad (12)$$

With the conditions  $V_r(r_a)=0$  and  $V_r(r_p)=0$ , one can find that the orbital parameters  $e$  and  $p$  can be written as a function of  $E$  and  $L_z$ , and vice versa. For an equatorial orbit, its orbital frequency is characterized by  $\Omega_r$  and  $\Omega_\phi$ , i.e.,

$$\Omega_r = \frac{2\pi}{T_r}, \quad \Omega_\phi = \frac{\Delta\phi}{T_r}. \quad (13)$$

Here the radial period  $T_r$  and the circumstellar shift  $\Delta\phi$  can be represented by simple integral expressions

[8, 9]

$$T_r = \int_{r_b}^{r_a} \frac{u^t}{u^r} dr = \int_0^{2\pi} \frac{dr}{d\chi} \frac{u^t}{u^r} d\chi, \quad (14)$$

$$\Delta\phi = \int_0^{T_r} \frac{u^\phi}{u^t} dt = \int_0^{2\pi} \frac{dr}{d\chi} \frac{u^\phi}{u^r} d\chi.$$

The number of cycles  $\mathcal{N}$  is a well quantity illustrated the difference between Kerr and swirling-Kerr orbits, which requires to accumulate difference  $\pi/2$  in periastron shift

$$\mathcal{N} = \frac{\pi/2}{|\Delta\phi_K - \Delta\phi_{sK}|}, \quad (15)$$

where the indices  $K$  and  $sK$  denote the Kerr and swirling-Kerr cases, respectively.

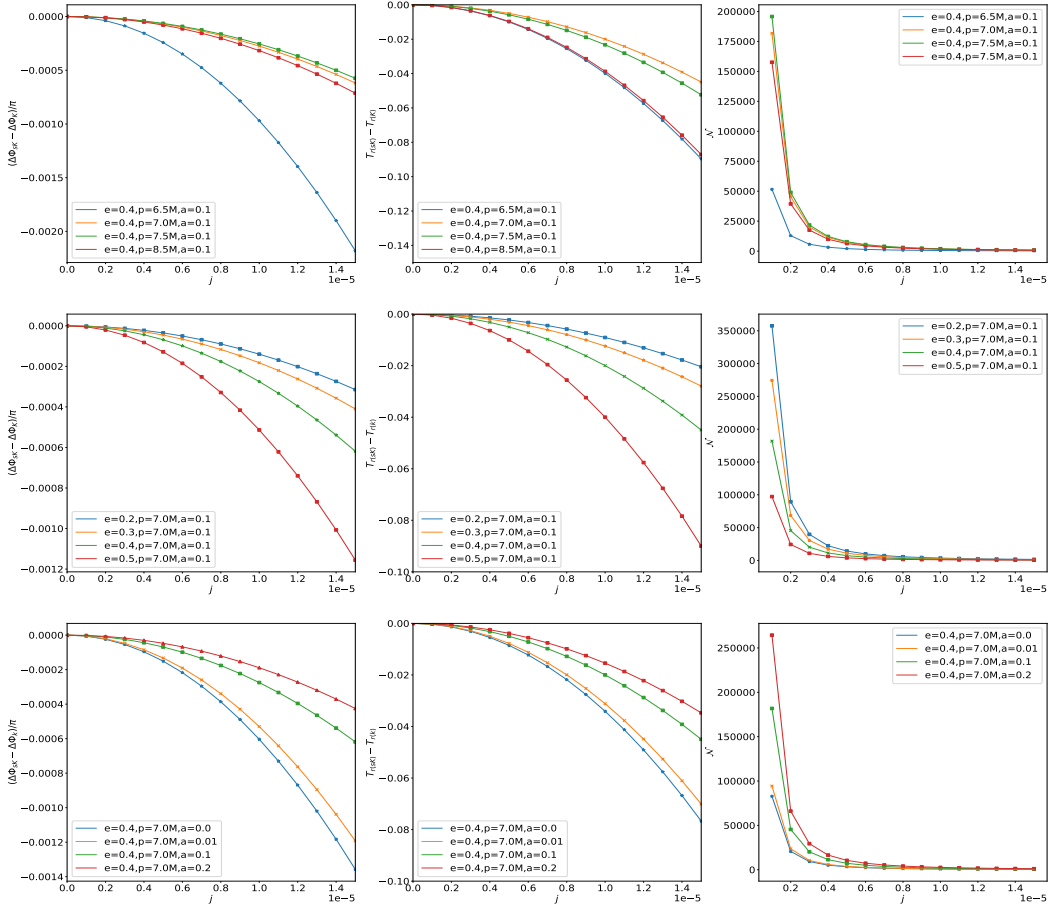


FIG. 1: Changes of the periastron shift difference  $\Delta\phi_{sK} - \Delta\phi_K$  (left panel), the radial period difference  $T_{r(sK)} - T_{r(K)}$  (middle panel) and the number of cycles  $\mathcal{N}$  (right panel) with the swirling parameter  $j$  for different  $e$ ,  $p$  and  $a$ .

The larger the number of cycles  $\mathcal{N}$  means the smaller orbital deviations. Figure 1 shows effects of orbital parameters  $e$ ,  $p$  and black hole spin  $a$  on the periastron shift difference  $\Delta\phi_{sK} - \Delta\phi_K$  (left panel), the radial period difference  $T_{r(sK)} - T_{r(K)}$  (middle panel) and the number of cycles  $\mathcal{N}$  for different swirling parameter  $j$ . Obviously, the absolute values of these orbital differences  $|\Delta\phi_{sK} - \Delta\phi_K|$  and  $|T_{r(sK)} - T_{r(K)}|$  increases with the swirling parameter  $j$ , while the number of cycles  $\mathcal{N}$  decreases. The effects of the parameters  $j$  is just opposite to those of the black hole spin parameter  $a$ , which could provide a probe to identify the swirling of the universe background. Moreover, with increases of the parameter  $p$ , the quantities  $|\Delta\phi_{sK} - \Delta\phi_K|$  and  $|T_{r(sK)} - T_{r(K)}|$  first decreases and then increases, while the number of cycles  $\mathcal{N}$  first increases and then decreases. With increase of the parameter  $e$ , the absolute values  $|\Delta\phi_{sK} - \Delta\phi_K|$  and  $|T_{r(sK)} - T_{r(K)}|$  increase and the number of cycles  $\mathcal{N}$  decreases.

We are now in position to compute the gravitational waveforms caused by the particle's trajectory in the swirling-Kerr spacetime with the kludge waveform generation method. As in Ref. [71], adopting Cartesian coordinates  $x = r \sin \theta \cos \phi$ ,  $y = r \sin \theta \sin \phi$ ,  $z = r \cos \theta$ , and employing the multipolar expansion of metric perturbations, one can obtain the lowest-order term in gravitational waves emitted by an isolated system through the quadrupole formula

$$\bar{h}^{jk}(t, x) = \frac{2}{R} [\ddot{I}^{jk}(t')]_{t'=t-r}, \quad (16)$$

where  $R$  denotes the luminosity distance from the source to the observer and  $I^{jk}(t')$  is the source's mass quadrupole moment with the form

$$I^{jk}(t') = \int x'^j x'^k T^{00}(t', x') d^3 x'. \quad (17)$$

Following the procedure proposed in Ref. [69, 70], with the transverse-traceless (TT) projection to the previously mentioned expressions and the standard TT gauge, the plus and cross components of the waveform observed at latitude  $\Theta$  and azimuth  $\Phi$  can be expressed as

$$\begin{aligned} h_+ &= h^{\Theta\Theta} - h^{\Phi\Phi} = \{\cos^2 \Theta [h^{xx} \cos^2 \Phi + h^{xy} \sin 2\Phi h^{yy} \sin^2 \Phi] + h^{zz} \sin^2 \Theta - \sin 2\Theta [h^{xz} \cos \Phi + h^{yz} \cos \Phi]\} \\ &\quad - [h^{xx} \sin^2 \Phi - h^{xy} \sin 2\Phi + h^{yy} \cos^2 \Phi], \\ h_\times &= 2h^{\Theta\Phi} = 2\{\cos \Theta [-\frac{1}{2} h^{xx} \sin 2\Phi + h^{xy} \cos 2\Phi + \frac{1}{2} h^{yy} \sin 2\Phi] + \sin \Theta [h^{xz} \sin \Phi - h^{yz} \cos \Phi]\}. \end{aligned} \quad (18)$$

To analyze the distinctions between waveforms in swirling Kerr spacetimes and those predicted from general relativity, we can utilize the overlap function to assess differences [9],

$$\mathcal{F}(\tilde{h}_1, \tilde{h}_2) = \frac{(\tilde{h}_1 | \tilde{h}_2)}{\sqrt{(\tilde{h}_1 | \tilde{h}_1)(\tilde{h}_2 | \tilde{h}_2)}}, \quad (19)$$

where the quantity marked with “tilde”  $\tilde{h}$  denotes the frequency domain signal related to the time domain signal  $h(t)$  of gravitational wave by the Fourier transforms. The inner product  $(\tilde{h}_1, \tilde{h}_2)$  is defined by [72–77]

$$(\tilde{h}_1 | \tilde{h}_2) = 2 \int_0^\infty \frac{\tilde{h}_1^*(f)\tilde{h}_2(f) + \tilde{h}_1(f)\tilde{h}_2^*(f)}{S_n(f)} df, \quad (20)$$

where  $S_n(f)$  is the signal-to-noise ratio of the detector. The noise spectral density of LISA is [74, 75]

$$S_n(f) = \frac{1}{L^2} \left\{ S_x + \left[ 1 + \left( \frac{0.4mHz^2}{f} \right) \frac{4S_a}{(2\pi f)^4} \right] \right\}. \quad (21)$$

The overlap function  $\mathcal{F}(\tilde{h}_1, \tilde{h}_2) = 1$  if the two waveforms are identical, while  $\mathcal{F}(\tilde{h}_1, \tilde{h}_2) = 0$  if they are totally uncorrelated, and  $\mathcal{F}(\tilde{h}_1, \tilde{h}_2) = -1$  if they are perfectly anti-correlated [10]. Therefore, the higher value of overlap function means that it is more difficult to distinguish these two waveform signals.

### III. EFFECTS OF THE SWIRLING PARAMETER ON EMRI GRAVITATIONAL WAVES

Let us now to probe effects of the swirling parameter together with the black hole spin parameter on EMRI gravitational waves using the numerical Kludge method. In our numerical analysis, the primary mass  $M$  and the secondary mass as  $\mu$  are respectively set as  $M = 2 \times 10^5 M_\odot$  (solar mass) and  $\mu = 2M_\odot$ , which means the mass ratio  $\eta = \mu/M = 10^{-5}$ . The observed angular parameters are set to  $\Theta = \pi/4$ ,  $\Phi = 0$ , and the luminosity distance is  $D_L = 5Gpc$ . To evaluate the effect of the rotation parameter  $j$  on the EMRI gravitational waves, we focus only on orbital evolutions on the equatorial plane, which are determined by conservative dynamics without explicitly considering radiative reactions.

The initial values of  $(E, L_z, Q)$  for the equatorial geodesic orbits in the context of conservative dynamics are given by [70]

$$V_r(E, L_z, Q = 0, r = r_a) = 0, \quad V_r(E, L_z, Q = 0, r = r_p) = 0, \quad Q = 0. \quad (22)$$

Taking the same initial positions and orbital parameters  $e$  and  $p$ , in Fig. 2, we present the time series of equatorially eccentric motion in the swirling Kerr black hole spacetime for different swirling parameter  $j$  over the first 2000 seconds. For fixed spin parameter  $a$ , we find that  $j$  significantly influences the orbit periods and phase. As  $j$  increases, the periods in the  $r$  direction is decrease and in the  $\phi$  direction increases. This observation is consistent with the results shown in Fig. 1. With increase of the spin parameter  $a$ , the influence of the swirling parameter  $j$  on the orbit decreases. As  $a$  increases up to  $a = 0.1$ , the difference arising from  $j$  is almost indistinguishable in both the  $r$  direction and  $\phi$  direction. This means that in the rapidly rotating



black hole case the effects of  $j$  can be negligible. These properties of the spacetime parameters on the geodesic orbital trajectories are also shown in the Fig. 3.

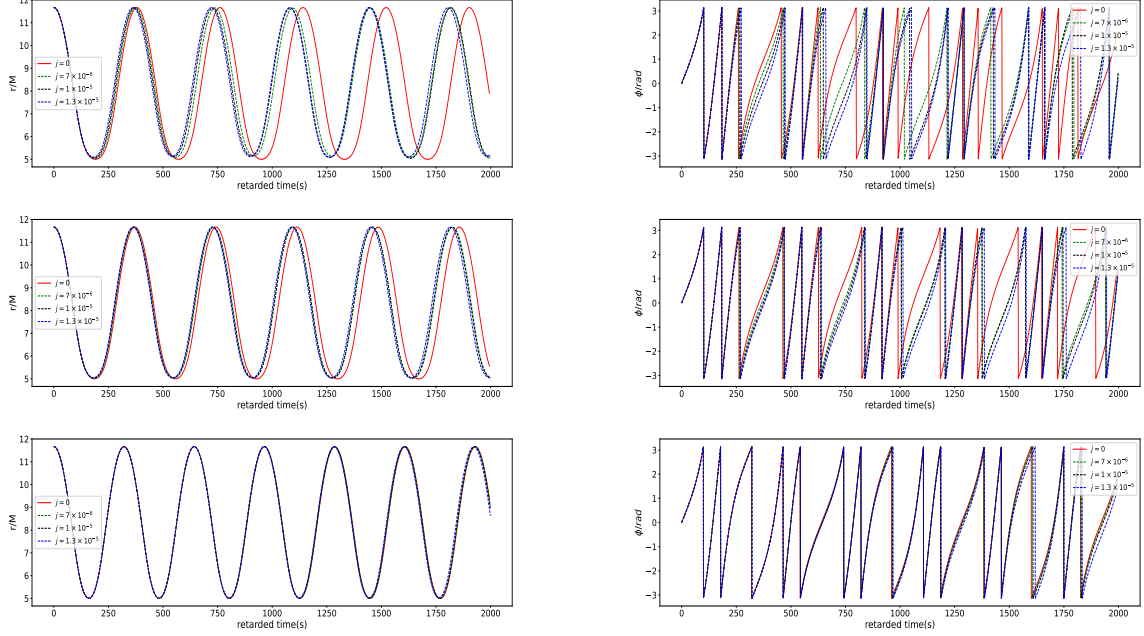


FIG. 2: Time series of the orbital motion with the orbital parameters  $e = 0.4$  and  $p = 7.0M$  in the swirling Kerr spacetime for different  $j$ . The left panel and the right panel respectively correspond to the motion in the  $r$ -direction and  $\phi$ -directions. The top, middle and bottom rows respectively denote  $a = 0.0$ ,  $a = 0.01$  and  $a = 0.1$ .

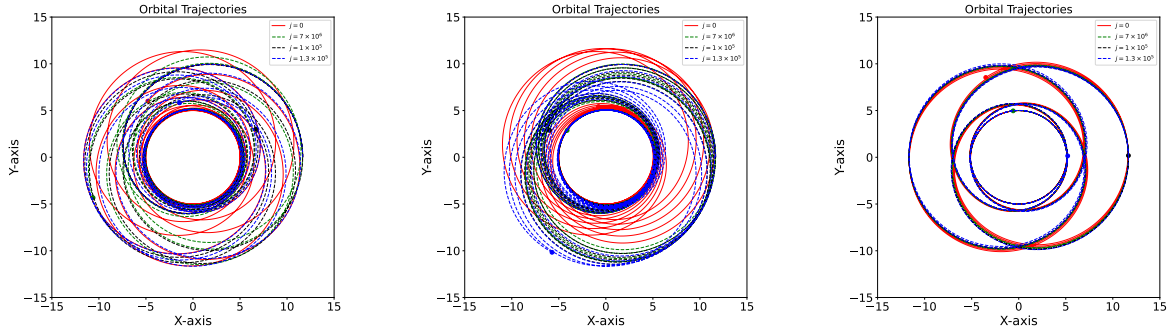


FIG. 3: Trajectories with the orbital parameters  $e = 0.4$  and  $p = 7.0M$  in the swirling Kerr spacetime for different swirling parameters  $j$ . The left, middle and right panels respectively correspond to cases  $a = 0$ ,  $a = 0.01$  and  $a = 0.1$ .

Based on the geodesic orbits given above, we can generate gravitational waveforms for plus and cross modes by using of the numerical Kludge method [69, 70], which are respectively shown in Figs. 4 and 5.

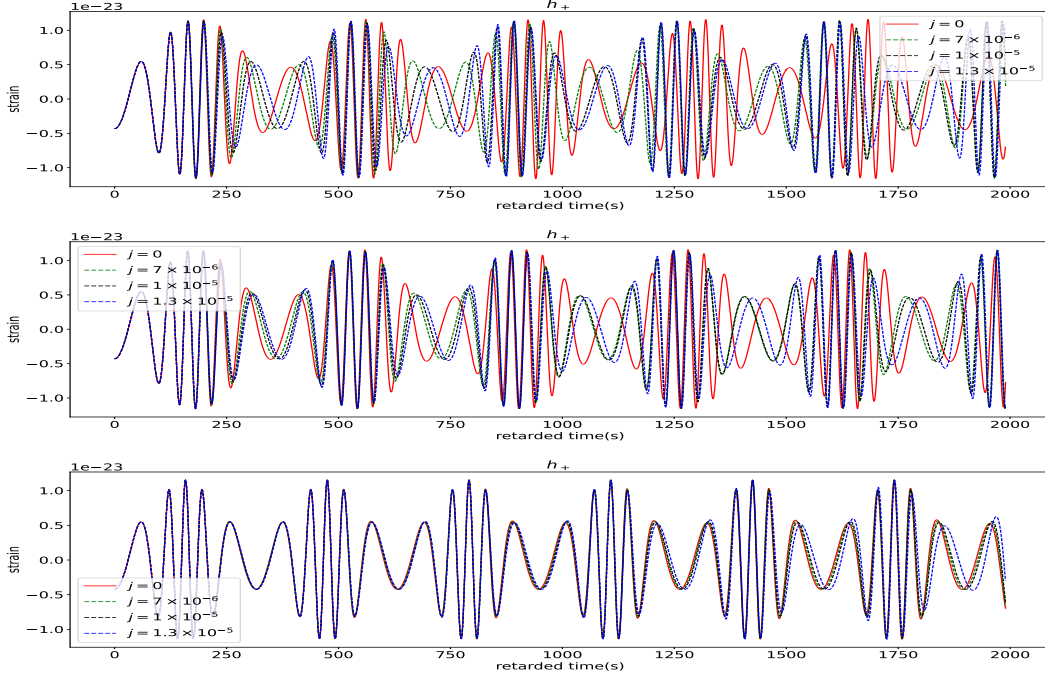


FIG. 4: The plus component of EMRI waveforms for different swirling parameter  $j$ . The top, middle and bottom rows respectively correspond to the cases with centre black hole's spin  $a = 0.0$ ,  $a = 0.01$ ,  $a = 0.1$ . Here, we set the orbital parameters to  $e = 0.4$  and  $p = 7.0M$ .

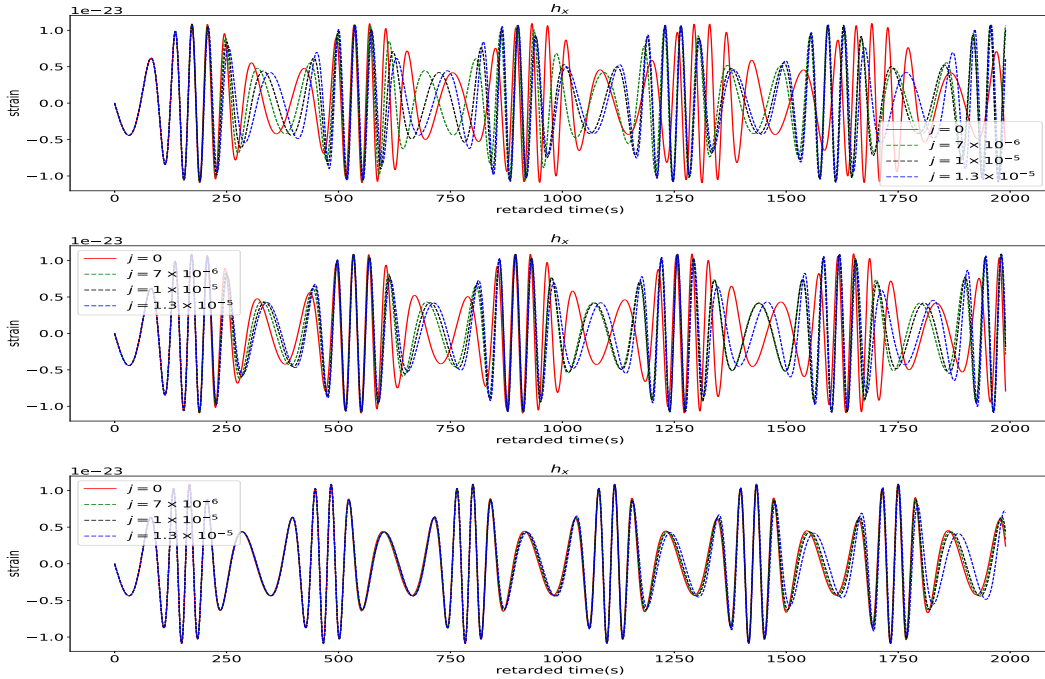


FIG. 5: The cross component of EMRI waveforms for different swirling parameter  $j$ . The top, middle and bottom rows respectively correspond to the cases with centre black hole's spin  $a = 0.0$ ,  $a = 0.01$ ,  $a = 0.1$ . Here, we set the orbital parameters to  $e = 0.4$  and  $p = 7.0M$ .

As  $a = 0$  and  $a = 0.01$ , we find that the parameter  $j$  has almost no effect on the gravitational waveforms

during the initial 200 seconds, while the impact of the parameter  $j$  becomes visually apparent after several orbital cycles and the parameter  $j$  causes a phase delay of gravitational waveforms. As  $a = 0.1$ , the gravitational waveform for different  $j$  is visually almost identical in the initial 500 seconds and distinct difference arising from  $j$  appear only after 1800 seconds. This means that the spin parameter  $a$  suppresses the effects of the swirling parameter  $j$  on the EMRI gravitational waves. Therefore, we can easily extract the information of the swirling parameter  $j$  from the EMRI gravitational waves in the slowly rotating black hole case. For the case with higher spin parameter, in order to distinguish between the Kerr orbital waveform and the swirling-Kerr orbital waveform, one can need the longer retarded time for the EMRI gravitational wave to accumulate effects from the swirling parameter  $j$ .

As in other cases, the confusion problem is encountered when one identifies the signal of the swirling parameter from the EMRI gravitational wave data observed by real detectors. The main reason is that there exists the possibility of significant overlap between the EMRI gravitational waveforms of Kerr and swirling-Kerr spacetimes as they share the same orbital frequency. The significant overlap makes it difficult to effectively distinguish between the waveforms in Kerr and swirling-Kerr cases. As in the previous discussion, we noted that the larger spin parameter leads to confusion problem where the effects of the swirling parameter  $j$  are heavily suppressed. In Fig.6, we present the orbital deviation between Kerr and swirling-Kerr spacetimes for the parameter set  $\{e, p, a\} = \{0.4, 7.0, 0.5\}$  for different  $j$  and find that the two orbits are almost indistinguishable in this case.

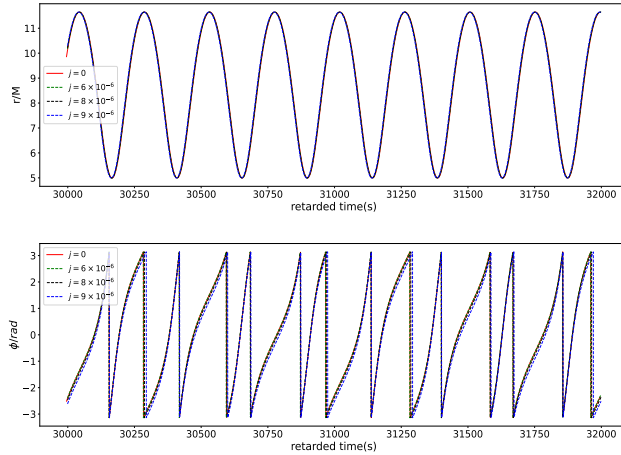


FIG. 6: Time series in the  $r$  and  $\phi$  directions under swirling-Kerr spacetime and Kerr spacetime with the same parameter set  $\{e, p, a\} = \{0.4, 7.0, 0.5\}$  for different swirling parameter  $j$ .

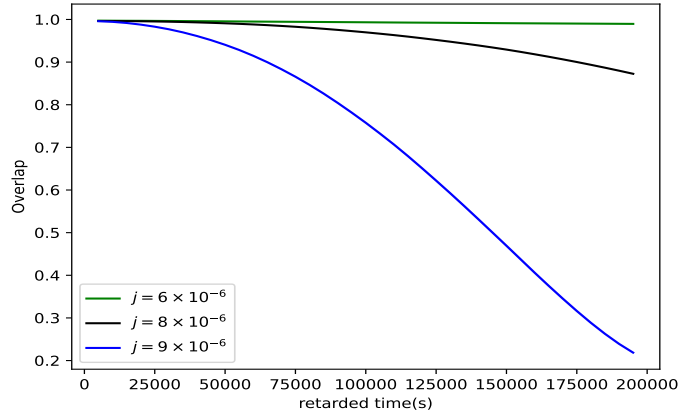


FIG. 7: The overlap as a function of retarded time  $t$  between Kerr and swirling-Kerr spacetimes with  $j = 6 \times 10^{-6}$  (green line),  $j = 8 \times 10^{-6}$  (black line) and  $j = 9 \times 10^{-6}$  (blue line). Here, the parameter set is  $\{e, p, a\} = \{0.4, 7.0, 0.5\}$ .

In Fig. 7, we also present the overlap with the retarded time  $t$  for  $j = 6 \times 10^{-6}$ ,  $8 \times 10^{-6}$  and  $9 \times 10^{-6}$ . We find that the overlap value for  $j = 6 \times 10^{-6}$  is still very high even if the retarded time  $t = 2 \times 10^5 s$ . This severely hinders our ability to detect the swirling parameter by analyzing EMRI gravitational waveforms.

Let us to discuss the possible confusion of gravitational waves induced by the orbital parameters  $e$  and  $p$ . As in ref.[10], one can calibrate the orbital frequency to look for combinations of parameters that might cause waveform confusion

$$\Omega_{ki}(j = 0, a_0, M_0, e_0, p_0) = \Omega_{si}(j, a_0, M_0, e_0 + \delta e, p_0 + \delta p), \quad i = r, \phi. \quad (23)$$

Here  $\delta p$  and  $\delta e$  are two small deviations of the orbital parameters. Solving above equations, we can obtain deviations  $\delta p$  and  $\delta e$  and further discuss confusion problem arising from orbital parameters  $e$  and  $p$  for fixed  $M$ ,  $a$  and  $j$ . In Fig. 8, we present the relationship between the relative variations of orbital parameters and  $j$  through matching the orbital frequency of Kerr and swirling-Kerr black holes. The results reveal that  $\delta e/e_0$  increases rapidly and  $\delta p/p_0$  decreases rapidly as  $j$  increases, which means that changes of the swirling parameter  $j$  must adjust the orbital parameters  $e$  and  $p$  to preserve consistent orbital frequencies. The change tendencies of  $\delta e/e_0$  and  $\delta p/p_0$  with the parameter  $j$  are similar to those with the MOG parameter  $\alpha$  [38], but the rates are different.

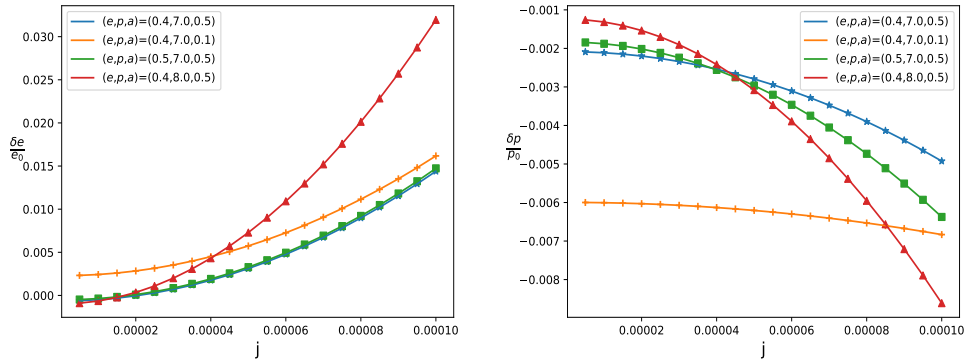


FIG. 8: Deviation in the orbital elements  $p$ ,  $e$  between Kerr (squares) and swirling-Kerr (circles) black holes after equating the orbital frequencies  $\Omega_r$ ,  $\Omega_\phi$ , and for fixed  $a = 0.5M$ ,  $j = 9 \times 10^{-6}$ .

Through above analysis, we find that the confusion problem also exists in the swirling-Kerr case. EMRI systems in the swirling-Kerr spacetime with different parameters cannot be distinguished from the corresponding Kerr black hole if their orbital frequencies are the same. The reason is that their EMRI waveforms are almost identical in this case.

#### IV. SUMMARY

Using the numerical Kludge scheme, we have studied the EMRI gravitational waves induced by eccentric orbits in the equatorial plane within the framework of the swirling-Kerr black hole spacetimes. In addition to the usual black hole mass and spin parameters, the swirling-Kerr black hole has an extra swirling parameter characterized the rotation of the universe background. We find that the swirling parameter  $j$  enhances the orbital differences between the swirling-Kerr black hole spacetime and the corresponding Kerr black hole spacetime, with effects opposite to those of the black hole spin parameter  $a$ . This distinction could serve as a potential probe for identifying the swirling of the universe background. As the parameter  $p$  increases, the quantities  $|\Delta\phi_{sK} - \Delta\phi_K|$  and  $|T_{r(sK)} - T_{r(K)}|$  initially decrease and then increase, while the number of cycles  $\mathcal{N}$  first increases and then decreases. On the other hand, as the orbital eccentricity  $e$  increases, the absolute values of  $|\Delta\phi_{sK} - \Delta\phi_K|$  and  $|T_{r(sK)} - T_{r(K)}|$  increase, while the number of cycles  $\mathcal{N}$  decreases.

For EMRI systems, the presence of the swirling parameter  $j$  results in a phase delay in the gravitational waveforms, while the black hole spin parameter  $a$  suppresses the impact of the swirling parameter  $j$  on the EMRI gravitational waves. As a result, extracting information about the swirling parameter  $j$  from the EMRI gravitational waves is much easier in the case of a slowly rotating black hole spacetime compared to a rapidly rotating black hole. Finally, we also analyze the confusion problem of gravitational waves in the swirling-

Kerr black hole spacetime. It is evident that a high black hole spin results in a significant overlap between waveforms for different values of the swirling parameter  $j$ . For instance, in the case  $a = 0.5$ , the overlap value for different  $j$  remains high even at a retarded time  $t = 2 \times 10^5 s$ . This significantly hinders our ability to detect the swirling parameter in the rapidly rotating black hole case by analyzing EMRI gravitational waveforms. Additionally, we explore the possible confusion of gravitational waves induced by the orbital parameters  $e$  and  $p$ . For EMRI gravitational waves with the same orbital frequencies, the allowable relative variations of orbital parameters  $\delta e/e_0$  increase rapidly, while  $\delta p/p_0$  decreases rapidly as  $j$  increases. The change trends of  $\delta e/e_0$  and  $\delta p/p_0$  with the parameter  $j$  are similar to those with the MOG parameter  $\alpha$ , but the rates are different. These results provide further insight into the properties of EMRI gravitational waves and the swirling of the universe background.

## V. ACKNOWLEDGMENTS

This work was supported by the National Natural Science Foundation of China under Grant No.12275078, 11875026, 12035005, 2020YFC2201400 and the innovative research group of Hunan Province under Grant No. 2024JJ1006.

- 
- [1] B. P. Abbott, et al. Observation of Gravitational Waves from a Binary Hole Merger. *Phy. Rev. Lett* **116**: 061102 (2016).
  - [2] B. P. Abbott, et al. GW170817: Observation of gravitational waves from a binary neutron star inspiral. *Phy. Rev. Lett* **119**: 161101(2017).
  - [3] B. P. Abbott, et al. Multi-messenger observations of a binary neutron star merger. *ApJL*. **848**: L12 (2017).
  - [4] J. R. Gair et al. Event rate estimates for LISA extreme mass ratio capture sources. *Class. Quant. Grav.* **21**, S1595 (2004), [arXiv:gr-qc/0405137](https://arxiv.org/abs/gr-qc/0405137).
  - [5] J. R. Gair and K. Glampedakis. Improved approximate inspirals of test bodies into Kerr black holes. *Phys. Rev. D* **73**, 064037(2006).
  - [6] S. A. Hughes. Evolution of circular, nonequatorial orbits of Kerr black holes due to gravitational-wave emission, II: Inspiral trajectories and gravitational waveforms. *Phys. Rev. D* **64**:064004(2001).
  - [7] S. Drasco and S. A. Hughes. Gravitational wave snapshots of generic extreme mass ratio inspirals. *Phys. Rev. D* **73**:024027(2006).
  - [8] K. Glampedakis and D. Kennefick. Zoom and whirl: Eccentric equatorial orbits around spinning black holes and their evolution under gravitational radiation reaction. *Phys. Rev. D* **66**, 044002(2002).
  - [9] K. Glampedakis and S. Babak. Mapping spacetimes with LISA: inspiral of a test body in a 'quasi-Kerr' field. [arxiv:gr-qc/0510057](https://arxiv.org/abs/gr-qc/0510057)

- [10] E. Barausse, L. Rezzolla, D. Petroff and M. Ansorg. Gravitational waves from extreme mass ratio inspirals in non-pure Kerr spacetimes. [arXiv:gr-qc/0612123](#)
- [11] E. A. Huerta and J. R. Gair. Influence of conservative corrections on parameter estimation for extreme-mass-ratio inspirals.[arXiv:0812.4208](#)
- [12] J. R. Gair et al. Forced motion near black holes. *Phys. Rev. D* **83**, 044037 (2011).
- [13] N. Warburton et al. Evolution of inspiral orbits around a Schwarzschild black hole. *Phys. Rev. D* **85**:061501(R)(2012).
- [14] C. Moreno-Garrido, E. Mediavilla and J. Buitrago. Gravitational radiation from point masses in elliptical orbits:spectral analysis and orbital parameters.*Mon. Not. R. Astron. Soc.* **274**,115-126(1995).
- [15] M. D. Hartl and A. Buonanno. Dynamics of precessing binary black holes using the post-Newtonian approximation. *Phys. Rev. D* **71**, 024027.
- [16] K. Glampedakis. Extreme mass ratio inspirals: Lisa’s unique probe of black hole gravity. [arXiv:gr-qc/0509024](#).
- [17] W. B. Han. Gravitational radiation from a spinning compact object around a supermassive kerr black hole in circular orbit. *Phys. Rev. D* **82**, 084013.
- [18] W. B. Han. Gravitational waves from extreme-mass-ratio inspirals in equatorially eccentric orbits.*Int. J. Mod. Phys. D*,23(07):1450064,2014.
- [19] W. B. Han.Fast evolution and waveform generator for extreme-mass-ratio inspirals in equatorial-circular orbits. [arXiv:1609.06817](#).
- [20] C. P. L. Berry, et al., [arXiv:1903.03686](#).
- [21] A. Torres-Orjuela, et al. Detection of astrophysical gravitational wave sources by TianQin and LISA. [arXiv:2307.16628](#).
- [22] LISA, P. Amaro-Seoane et al., Laser Interferometer Space Antenna, (2017), [arXiv:1702.00786](#).
- [23] K. Danzmann, *Class. Quant. Grav.* **14**, 1399 (1997).
- [24] W. Hu and Y. Wu, *Natl. Sci. Rev.* **4**, 685 (2017).
- [25] Y. Gong, J. Luo, and B. Wang, *Nature Astron.* **5**, 881 (2021), [arXiv:2109.07442](#).
- [26] TianQin, J. Luo et al., *Class. Quant. Grav.* **33**, 035010 (2016), [arXiv:1512.02076](#).
- [27] E. Barausse et al. Prospects for Fundamental Physics with LISA. [arXiv:2001.09793](#).
- [28] P. A. Seoane et al. Astrophysics with the Laser Interferometer Space Antenna. [arXiv:2203.06016](#).
- [29] K. G. Arun et al. New horizons for fundamental physics with LISA. [arXiv:2205.01597](#).
- [30] N. Karnesis et al. The Laser Interferometer Space Antenna mission in Greece White Paper. [arXiv:2209.04358](#).
- [31] J. R. Gair, M. Vallisneri, S. L. Larson and J. G. Baker. Testing general relativity with low-frequency,space-based gravitational-wave detectors. [arXiv:1212.5575v2](#).
- [32] G. A. Piovano, A. Maselli, and P. Pani, *Phys. Lett. B* **811**, 135860 (2020), [arXiv:2003.08448](#).
- [33] S. Datta and S. Bose, *Phys. Rev. D* **99**, 084001 (2019), [arXiv:1902.01723](#).
- [34] A. G. Shah, J. L. Friedman, and T. S. Keidl, *Phys. Rev. D* **86**, 084059 (2012), [arXiv:1207.5595](#).
- [35] S. Xin, W. Han, and S. Yang,*Phys. Rev. D* **100**, 084055 (2019), [arXiv:1812.04185](#).
- [36] E. Berti, A. Buonanno, and C. M. Will, *Class. Quant. Grav.* **22**, S943 (2005), [arXiv:gr-qc/0504017](#).
- [37] N. Yunes, P. Pani, and V. Cardoso, *Phys. Rev. D* **85**, 102003 (2012), [arXiv:1112.3351](#).
- [38] X. Qiao, Z. Xia, Q. Pan, H. Guo, W. Qian, J. Jing,[arXiv:2408.10022](#) .
- [39] C. F. Sopuerta and N. Yunes, *Phys. Rev. D* **80**, 064006 (2009), [arXiv:0904.4501](#).



- [40] P. Pani, V. Cardoso, and L. Gualtieri, *Phys. Rev. D* **83**, 104048 (2011), [arXiv:1104.1183](#).
- [41] P. Canizares, J. R. Gair, and C. F. Sopuerta, *Phys. Rev. D* **86**, 044010 (2012), [arXiv:1205.1253](#).
- [42] S. Yang, Y. Zhang, T. Zhu, L. Zhao, and Y. Liu, [arXiv:2412.04302](#).
- [43] T. Zi, S. Kumar, [arXiv:2409.17765](#).
- [44] G. Fu, Y. Liu, B. Wang, J. Wu, C. Zhang, [arXiv:2409.08138](#).
- [45] C. F. B. Macedo, P. Pani, V. Cardoso, and L. C. B. Crispino, *Astrophys. J.* **774**, 48 (2013), [arXiv:1302.2646](#).
- [46] O. A. Hannuksela, K. C. Y. Ng, and T. G. F. Li, *Phys. Rev. D* **102**, 103022 (2020), [arXiv:1906.11845](#).
- [47] N. Dai, Y. Gong, Y. Zhao, and T. Jiang, (2023), *Phys. Rev. D* **110**, 084080 (2024), [arXiv:2301.05088](#).
- [48] A. Maselli, N. Franchini, L. Gualtieri, and T. P. Sotiriou, *Phys. Rev. Lett.* **125**, 141101 (2020), [arXiv:2004.11895](#).
- [49] A. Maselli et al., *Nature Astron.* **6**, 464 (2022), [arXiv:2106.11325](#).
- [50] H. Guo et al., *Phys. Rev. D* **106**, 024047 (2022), [arXiv:2201.10748](#).
- [51] Y. P. Zhang et al., [arXiv:2108.13170](#).
- [52] S. Barsanti, N. Franchini, L. Gualtieri, A. Maselli, and T. P. Sotiriou, *Phys. Rev. D* **106**, 044029 (2022), [arXiv:2203.05003](#).
- [53] C. Zhang, Y. Gong, D. Liang, and B. Wang, *JCAP* **06**, 054 (2023), [arXiv:2210.11121](#).
- [54] H. Guo, et al., *Chin. Phys. C* **48**, 095103 (2024), [arXiv:2305.00652](#).
- [55] S. Barsanti, A. Maselli, T. P. Sotiriou, and L. Gualtieri, *Phys. Rev. Lett.* **131**, 051401 (2023), [arXiv:2212.03888](#).
- [56] T. Zi et al., *Phys. Rev. D* **107**, 023005 (2023), [arXiv:2205.00425](#).
- [57] D. Liang, R. Xu, Z. F. Mai, and L. Shao, *Phys. Rev. D* **107**, 044053 (2023), [arXiv:2212.09346](#).
- [58] C. L. MacLeod and C. J. Hogan. Precision of Hubble constant derived using black hole binary absolute distances and statistical redshift information. *Phys. Rev. D* **77**, 043512(2008).
- [59] M. Astorino, R. Martelli and A. Vigan. Black holes in a swirling universe. *Phys. Rev. D* **106**, 064014(2022).
- [60] F. J. Ernst. New Formulation of the Axially Symmetric Gravitational Field Problem. *Phys. Rev.* **167**, 1175(1968).
- [61] F. J. Ernst. New Formulation of the Axially Symmetric Gravitational Field Problem.II. *Phys. Rev.* **168**, 1415(1968).
- [62] D. Cao, L. Zhang, S. Chen, Q. Pan, J. Jing, [arXiv:2410.03214](#).
- [63] R. Capobianco, B. Hartmann, and J. Kunz, [arXiv:2312.17347](#).
- [64] Z. S. Moreira, C. A. R. Herdeiro, and L. C. B. Crispino, [arXiv:2401.05658](#).
- [65] C. Chen, Q. Pan, and J. Jing, *Eur. Phys. J. C* **84**(10), 1040 (2024), [arXiv:2402.02789](#).
- [66] K. Gjorgjeski and R. Capobianco, [arXiv:2405.16758](#).
- [67] J. Barrientos et al. Mixing “Magnetic” and “Electric” Ehlers-Harrison transformations: the electromagnetic swirling spacetime and novel type I backgrounds. [arXiv:2401.02924](#).
- [68] J. Barrientos, A. Cisterna, M. Hassaine and K. Pallikaris. Electromagnetized Black Holes and Swirling Backgrounds in Nonlinear Electrodynamics: The ModMax case. [arXiv:2409.12336](#).
- [69] S. Babak, H. Fang, J. R. Gair, K. Glampedakis and S. A. Hughes. Kludge gravitational waveforms for a test-body orbiting a Kerr black hole. *Phys. Rev. D* **75**, 024005(2007).
- [70] A. J. K. Chua, C. J. Moore and J. R. Gair. Augmented kludge waveforms for detecting extreme-mass-ratio inspirals. *Phys. Rev. D* **96**, 044005(2017).
- [71] K. S. Thorne. Multipole expansions of gravitational radiation. *Rev. Mod. Phys.* **52**, 299.
- [72] L. Barack and C. Cutler. LISA Capture Sources: Approximate Waveforms, Signal-to-Noise Ratios and Parameter Estimation Accuracy. *Phys. Rev. D* **69**, 082005(2004).



- [73] L. S. Finn. Detection, Measurement and Gravitational Radiation. *Phys. Rev. D* **46**, 5236(1992).
- [74] T. Robson, N. Cornish and C. Liu. The construction and use of LISA sensitivity curves. [arXiv:1803.01944](#)
- [75] S. Babak, M. Hewitson, A. Petiteau. LISA Sensitivity and SNR Calculations. [arxiv:2109.01167](#).
- [76] C. Cutler and E. Flanagan. Gravitational Waves from Merging Compact Binaries: How Accurately Can One Extract the Binary's Parameters from the Inspiral Waveform? *Phys. Rev. D* **49**,2658(1994).
- [77] R. Balasubramanian, B. S. Sathyaprakash and S. V. Dhurandhar. Gravitational waves from coalescing binaries: detection strategies and Monte Carlo estimation of parameters. *Phys. Rev. D* **53**,3033(1996).